Comparison Between Parallel Hole and Rotating Slat Collimation

Lin Zhou, Michel Defrise, Kathleen Vunckx and Johan Nuyts

***Abstract*— In this study, we compared the performance of parallel hole (PH) and rotating slat (RS) collimations at equal spatial resolution. Based on mathematical calculations, we derived the linear relationship between the optimal collimator aperture and the target spatial resolution for each collimator, and calculated the gain in signal-to-noise ratio (RS over PH) for the central point of a homogeneous symmetrical phantom using these optimized collimator parameters. These results were supported by an efficient analytical Fisher information-based method. The collimations were compared for both planar imaging and volume imaging. The main results are: 1) For the same target resolution, the optimal system resolution depends on the collimator and the imaging mode (planar or volume). 2) RS has lower variance than PH when the object is smaller than the detector.**

I. Introduction

In single photon emission computed tomography (SPECT) imaging, image quality is always limited by the tradeoff between the spatial resolution and the system sensitivity. In contrast to the conventional parallel hole (PH) geometry, a rotating slat (RS) collimation can overcome this limitation by a much higher photon collection efficiency [1]. However RS has the drawback of increased noise propagation. The goal of our study is to compare PH and RS to see which collimator provides better image quality.

To compare PH and RS fairly, we imposed a matched target spatial resolution for the reconstruction image. As we fixed the target resolution (TR), the variance (Var) in the reconstruction image varies with the aperture of the collimator. We introduced a concept of "optimal collimator aperture" which is defined as the one that corresponds to the minimal variance in the reconstructions. In this study we investigated the relationship between the optimal collimator aperture and the target resolution for each collimator, and used these optimized parameters for the further comparison between PH and RS.

We mainly use two approaches for investigation. The first one is an analytic calculation based on filtered-backprojection (FBP) reconstruction, similar to the work by Lodge [2], [3]. The main goal of this paper is to compare this analytic approach to an alternative approach based on the calculation of the linearized impulse response and of the covariance, using the Fisher information matrix [4]–[6]. The comparison is done for a very simple physical model of the PH and of the RS collimators, but, once validated, the Fisher information-based method could easily be extended to more sophisticated models including for instance the distance-dependence of the collimator resolution.

L.Zhou, K.Vunckx and J.Nuyts are with the Dept. of Nuclear Medicine, K.U.Leuven, B-3000 Leuven, Belgium. M.Defrise is with the Dept. of Nuclear Medicine, V.U.Brussel, B-1090 Brussel, Belgium

This work is supported by F.W.O. grant G.0569.08. and I.U.A.P. grant NIMI.

II. Methods

A. FBP Calculation

For this analytical calculation, the central point in a homogeneous symmetrical object (disk or sphere) is studied using FBP for image reconstruction. For the ideal object and the imaging system studied, FBP yields the unweighted least squares (LS) solution. However, for the central point the result should be very similar to the weighted least squares (WLS) solution, since the relevant weights are nearly equal because of the symmetry.

Fig. 1 and 2 show the flow charts of the FBP calculation for planar imaging and volume imaging, respectively. For planar imaging, the calculation starts from a 2D flat disk phantom $f(\vec{x})$ ($\vec{x} \in \mathbb{R}^2$) positioned parallel to the surface of the detector array. PH collimator is stationary while RS spins around its central axis in order to obtain the complete data. E is the geometric efficiency and T is the acquisition time. The subscript p and r represent PH and RS, respectively.

We model the PH measurements as a convolution between $f(\vec{x})$ and a 2D Gaussian point spread function (PSF) with standard deviation σ_p. The measurement of RS is described as a convolution between the ideal 2D Radon transform of $f(\vec{x})$ and a 1D Gaussian PSF with standard deviation σ_r. Here we use σ_p and σ_r to roughly model the collimator apertures. To reconstruct the image, the PH data need to be deblurred for the effect of collimator smoothing, and then be smoothed again by the fixed target resolution σ_t. For RS, we process the data in the same way as for PH, and then apply FBP. For the image quality, the signal-to-noise ratio (SNR) is used as figure of merit.

The variance in the reconstuction is a function of σ_p (PH) or σ_r (RS), therefore the optimal σ_p and σ_r can be found by minimizing the variance for both collimators. With the optimal collimator parameter, the performance of PH and RS can be fairly compared by calculating the optimized SNR gain ($\mathrm{SNR_{RS}}/\mathrm{SNR_{PH}}$) at a matched spatial resolution.

The calculation for volume imaging is quite similar. In this case, the collimator and the detector rotate around a 3D uniform spherical phantom $f(\vec{x})$. The measurement can be modeled as a 2D (PH) or 3D (RS) Radon transform of $f(\vec{x})$ followed by the smoothing effect of σ_p or σ_r. Proper filters are applied in the image reconstruction. All the rest is just the same as for the planar imaging.

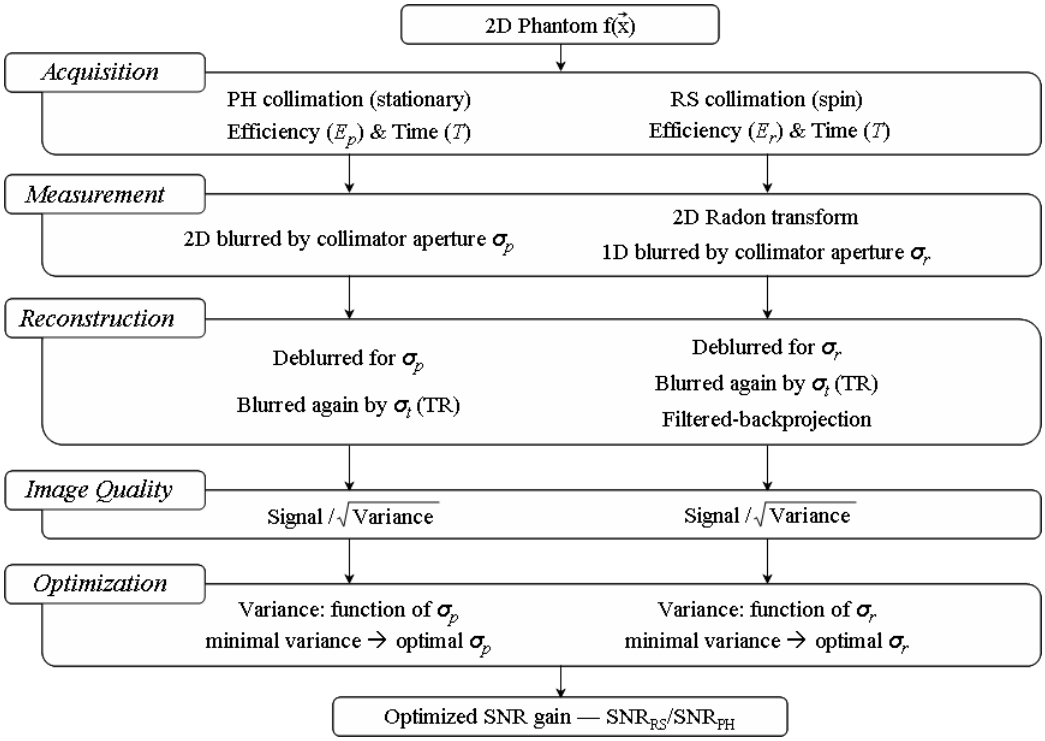

Fig. 1. FBP calculation procedure for planar imaging.

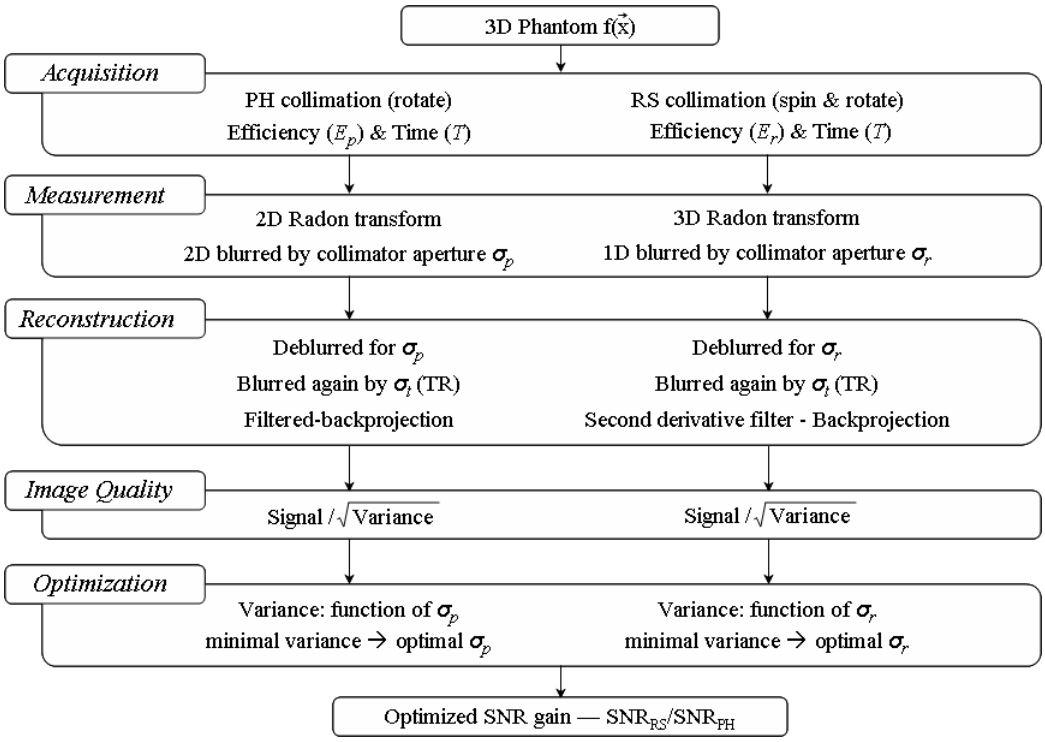

Fig. 2. FBP calculation procedure for volume imaging.

In the FBP calculation we made several approximations, therefore this method is only valid for the central point of a symmetrical phantom. A detailed explanation for the calculation can be found in Appendix.

B. Fisher Information-Based Method

Fisher information-based method (FIM) is an efficient analytical method which predicts the linearized local impulse response (LLIR) and the covariance in one reconstruction pixel. FIM was first proposed in [4], [5] for converged maximum-a-posteriori (MAP) reconstruction. Later it was adapted and validated in [6] for post-smoothed maximum likelihood expectation maximization (MLEM) with a desired target resolution:

$$l^j(\Lambda) \approx \boldsymbol{P}^j \boldsymbol{G}^j \boldsymbol{F}^j e^j \tag{1}$$

$$\mathrm{Cov}^j(\Lambda) \approx \boldsymbol{P}^j \boldsymbol{G}^j \boldsymbol{F}^j \boldsymbol{G}^{jT} \boldsymbol{P}^j e^j \tag{2}$$

where Λ is the reconstruction image, j is the pixel index in the reconstruction, $l^j(\Lambda)$ and $\mathrm{Cov}^j(\Lambda)$ are the LLIR and the covariance image of pixel j, i.e., the k-th element of $\mathrm{Cov}^j(\Lambda)$ is the covariance between the reconstructed pixels j and k. Λ, $l^j(\Lambda)$ and $\mathrm{Cov}^j(\Lambda)$ are in $\mathbb{R}^N$, with N the number of pixels. $\boldsymbol{P}^j$ is an isotropic Gaussian post-smooth filter that tries to impose the given target resolution and $\boldsymbol{G}^j$ is the approximate pseudoinverse of the Fisher information matrix $\boldsymbol{F}^j$, ^{T} denotes transpose. All factors are j-dependent due to the assumption of local shift-invariance.

The j-th element of $l^j(\Lambda)$ and $\mathrm{Cov}^j(\Lambda)$ are the contrast recovery coefficient (CRC) and the variance in pixel j, respectively. With FIM, the contrast-to-noise ratio (CNR) is used as the image quality measure, which is defined as:

$$\mathrm{CNR} = \mathrm{CRC}/\sqrt{\mathrm{Var}} \tag{3}$$

The validation of Eq. (1) and (2) can be done by doing repeated simulations using post-smoothed MLEM reconstruction algorithm. In our study, we did the validation for both PH and RS collimator systems for planar imaging. Given a certain pixel j, the LLIR can be obtained by reconstructing the projection data of the phantom with and without an impulse at j. The covariance image can be calculated from the reconstructions of a large number of noisy projection data sets. With both FIM and simulation, we calculated the CRC and the variance for various points of different phantoms. The CRC and the variance predicted by FIM were always in good accordance with the simulation results (not shown in this paper).

For a given target resolution, CRC is constant if the shape of the LLIR is Gaussian (which is the case in our study). Meanwhile, the variance is a function of the collimator aperture, which can be modeled in the projection/back-projection matrix. With FIM, the optimal collimator aperture was found by the following steps: 1) Plot the CNR curve as function of collimator aperture. 2) Fit the curve by the least-squares polynomial fitting method. 3) Locate the maximal CNR on the curve. 4) Define the collimator aperture which corresponds to the maximal CNR as the optimal collimator aperture.

The SNR gain and CNR gain of RS over PH are derived as follows:

$$\mathrm{Gain}_{\mathrm{SNR}} = \frac{\mathrm{SNR}_{\mathrm{RS}}}{\mathrm{SNR}_{\mathrm{PH}}} = \frac{\mathrm{Signal}_{\mathrm{RS}}/\sqrt{\mathrm{Var}_{\mathrm{RS}}}}{\mathrm{Signal}_{\mathrm{PH}}/\sqrt{\mathrm{Var}_{\mathrm{PH}}}} \tag{4}$$

$$\mathrm{Gain}_{\mathrm{CNR}} = \frac{\mathrm{CNR}_{\mathrm{RS}}}{\mathrm{CNR}_{\mathrm{PH}}} = \frac{\mathrm{CRC}_{\mathrm{RS}}/\sqrt{\mathrm{Var}_{\mathrm{RS}}}}{\mathrm{CRC}_{\mathrm{PH}}/\sqrt{\mathrm{Var}_{\mathrm{PH}}}} \tag{5}$$

For the same phantom and the same target resolution, we should have $\mathrm{Signal}_{\mathrm{PH}} = \mathrm{Signal}_{\mathrm{RS}}$, and $\mathrm{CRC}_{\mathrm{PH}} = \mathrm{CRC}_{\mathrm{RS}}$. Then (4) and (5) become equivalent:

$$\mathrm{Gain}_{\mathrm{SNR}} = \mathrm{Gain}_{\mathrm{CNR}} = \sqrt{\frac{\mathrm{Var}_{\mathrm{PH}}}{\mathrm{Var}_{\mathrm{RS}}}} \tag{6}$$

As argued above, the FBP calculation predicts the variance of the LS reconstruction near the center of a symmetrical object. However, for a large symmetrical object, most of the sinogram values contributing to the reconstruction of a central point have the same value. Due to the Poisson distribution, they also have the same variance, which means that LS can be approximately considered as WLS. On the other hand, the approximate Fisher information-based method yields predictions that are in good agreement with reconstructions produced with MLEM or WLS followed by post-smoothing. Therefore, for a large symmetrical object, post-smoothed LS, WLS and MLEM should all produce nearly the same variance at matched resolution. Consequently, FBP calculation and FIM should agree well for these central points. However, FIM is more accurate and can be applied to arbitrary, non-uniform distributions as well, therefore we use FIM to generalize the results of the FBP calculation.

C. Parameter Settings

1) Phantom: In our study we used 2D homogeneous disk phantoms for planar imaging, and 3D homogeneous spherical phantoms for volume imaging.

2) System Parameters: Table I shows the system parameters used for FIM. Thickness of the collimator septa was not modeled. Detector efficiency was assumed perfect. The acquisition time for the two systems was kept the same. For the volume imaging, distance-dependent blurring was not modeled. Instead, a constant resolution corresponding to the central location of the phantom was used.

3) Collimator Aperture: We defined the collimator aperture as:

$$\sigma = \frac{\mathrm{FWHM}}{\sqrt{8\ln 2}} = \frac{Dd}{\sqrt{8\ln 2}h} \tag{7}$$

where FWHM (full width at half maximum) represents the system resolution defined by the collimator geometry, D is the distance between the centre of the phantom and the detector, d is the distance between the PH or RS collimator septa, and h is the height of the collimator septa.

For PH and RS, we fixed D and d, and only varied h to adapt the collimator aperture σ_p and σ_r.

TABLE I

SYSTEM PARAMETERS FOR FISHER INFORMATION-BASED METHOD

Parameter	Planar imaging	Volume imaging
Detector array	128x128	64x64
Image space	128x128	64x64x64
Pixel size	1.8mm	1.8mm
Projection angles	PH: stationary RS: 128 spin angles over 2π	PH: 60 rotation angles over 2π RS: 60 spin / 60 rotation angles over 2π

4) Effective Detector Width: For RS, less photons are detected at the edge than at the centre of the detector. Therefore we introduced a concept of effective detector width Ω_W. For the central point of the phantom, Ω_W is defined as:

$$\Omega_W = \int_{-W/2}^{+W/2} \cos^3 \beta(x) dx \tag{8}$$

W is the width of the detector along the slat collimator septa. β is the angle between the trajectory of the photon (emitted from the central point of the phantom and detected at a location on the detector) and the normal to the detector, hence:

$$\beta(x) = \arctan \frac{x}{D}, \quad x \in [-W/2, W/2] \tag{9}$$

When $D >> W$, $\Omega_W \approx W$ (See Appendix-A).

III. RESULTS

A. Results from FBP Calculation

For the central point of a homogeneous symmetrical phantom, we obtained a linear relationship between the target resolution σ_t and the optimal collimator apertures σ_p^{opt}, σ_r^{opt}. For planar imaging:

$$\sigma_p^{opt} = \sigma_t/\sqrt{2} \tag{10}$$

$$\sigma_r^{opt} = \sigma_t/2 \tag{11}$$

and for volume imaging:

$$\sigma_p^{opt} = \sigma_t/\sqrt{3} \tag{12}$$

$$\sigma_r^{opt} = \sigma_t/\sqrt{6} \tag{13}$$

With these optimal collimator apertures, we calculated the minimal variance for PH and RS for a fixed target resolution σ_t, and derived expressions for the SNR gain for both planar imaging and volume imaging:

$$\text{Gain}_{\text{SNR}}^{\text{opt}}(\text{planar}) = 1.116\sqrt{\frac{\Omega_W}{diameter}} \tag{14}$$

$$\text{Gain}_{\text{SNR}}^{\text{opt}}(\text{volume}) = 1.192\sqrt{\frac{\Omega_W}{diameter}} \tag{15}$$

where $diameter$ refers to the diameter of the phantom.

If $D >> W$, we have $\Omega_W \approx W$ (See Appendix-A), and Eq. (14) and (15) become:

$$\text{Gain}_{\text{SNR}}^{\text{opt}}(\text{planar}) = 1.116\sqrt{\frac{W}{diameter}} \tag{16}$$

$$\text{Gain}_{\text{SNR}}^{\text{opt}}(\text{volume}) = 1.192\sqrt{\frac{W}{diameter}} \tag{17}$$

Eq. (16) and (17) imply that in the far-field case, RS is always better than PH as long as the phantom diameter is smaller than the detector array.

B. Comparison with FIM

Fig. 3 compares the results of FBP calculation (Eq. (10), (11)) and the results of FIM for planar imaging. Fig. 3(a) shows the 2D disk phantom and the points of interest. Fig. 3(b) plots the relationship between the optimal collimator aperture and the target resolution for the central point of the phantom. For FBP/FIM, the cross/diamond and plus/asterisk symbols represent PH and RS, respectively. The curves of two methods coincide. Fig. 3(c) shows the optimal aperture for all points of interest (0-4) calculated by FIM for a fixed target resolution. From Fig. 3(b) and Fig. 3(c) we can see that Eq. (10) and (11) correctly predict the FIM results for both central point and eccentric points of a homogeneous symmetrical phantom. Fig. 3(d) shows the CNR of all the points which were calculated based on the optimized collimator parameters. For points towards the edge of the phantom, CNR_{PH} remains unchanged and CNR_{RS} increases.

Fig. 4 shows the CNR(SNR) gain which was plotted as function of detector distance D or phantom diameter. We can see that Eq. (14) is in good agreement with FIM for small phantoms (Fig. 4(a)) and large D (Fig. 4(c)). However, for large phantoms (Fig. 4(b)) or small D (Fig. 4(d)), the CNR(SNR) gain is underestimated by Eq. (14).

Fig. 5 plots the relationship between the optimal aperture and the target resolution for volume imaging. The results are plotted for different phantom sizes. Based on the result from FBP calculation, the optimal aperture only varies with the target resolution and is diameter-independent. However, FIM shows that the relationship is additionally influenced by the phantom size. Eq. (12) and (13) are more accurate for larger phantoms.

Fig. 6 shows the results for all points of interest in volume imaging. In Fig. 6(a), the points are selected along/perpendicular to the axis of rotation. Fig. 6(b) plots the optimal aperture for every point calculated by two methods for a fixed target resolution. The dashed lines plot the FBP values of the central point as reference. From these plots we can see that PH is almost shift-invariant, while RS is more shift-variant, especially along the axis of rotation. Fig. 6(c) shows the optimized CNR of all points of interest. Here we still use Eq. (12) and (13) as the definition of the optimal collimator

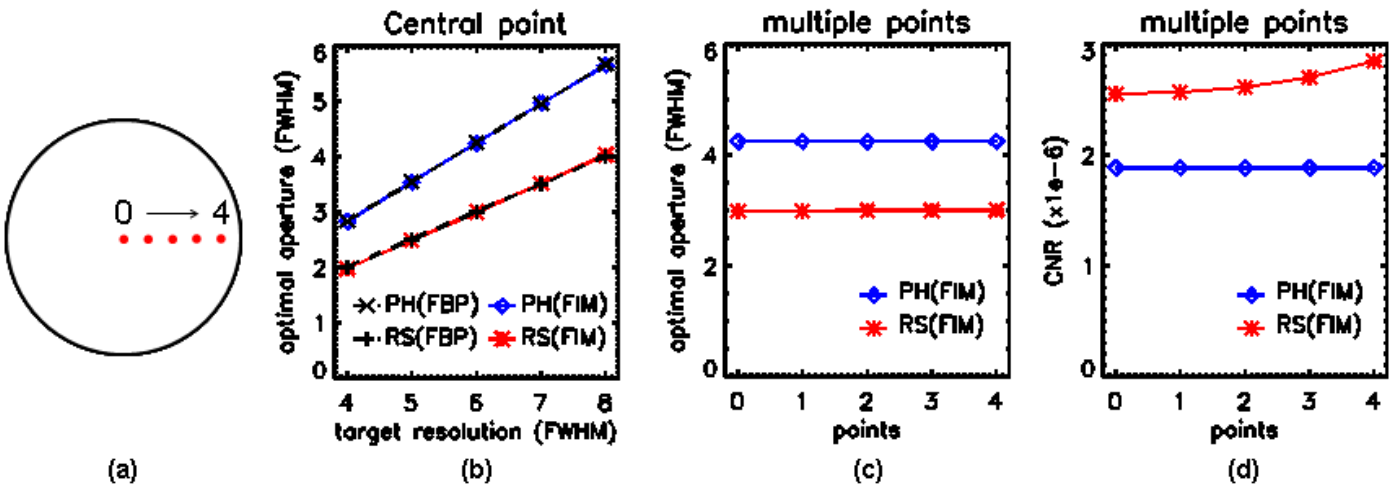

Fig. 3. Comparison between FBP (Eq. (10), (11)) and FIM for planar imaging. (a) Disk phantom and points of interest. 0 is the central point and 4 is the most eccentric point. (b) Plot of optimal aperture as function of target resolution by two methods. (c) Optimal aperture for all points of interest for a fixed target resolution ($\text{FWHM}_t = 6pix$). (d) CNR of all points of interest with optimized collimator parameters.

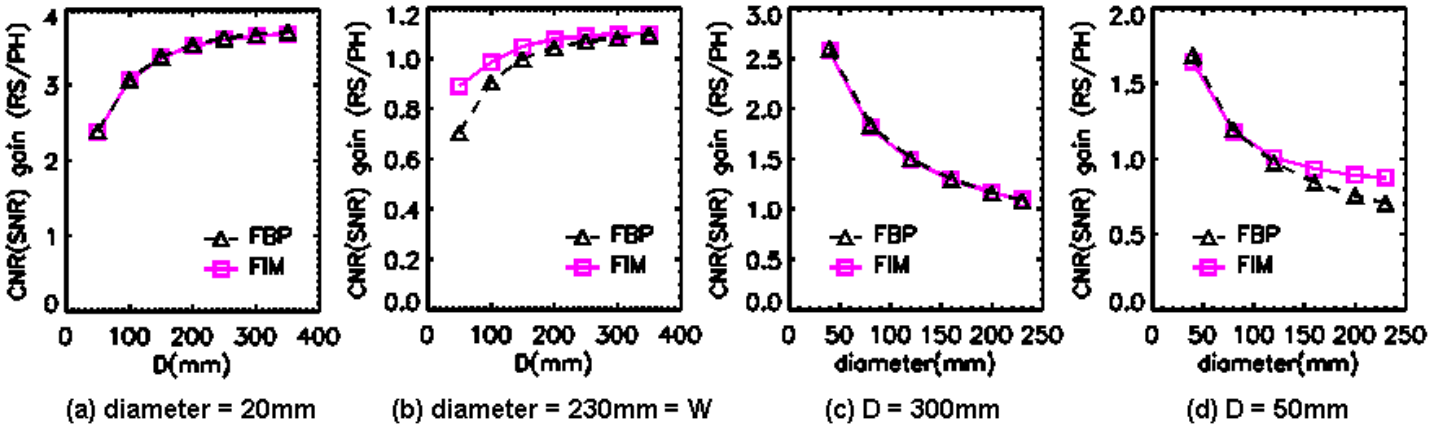

Fig. 4. Comparison between FBP (Eq. (14)) and FIM for planar imaging. (a) CNR(SNR) gain as function of detector distance D for the central point in a small phantom (diameter = 20mm). (b) Same as (a), but for a large phantom (diameter = 230mm = W). (c) CNR(SNR) gain as function of phantom size at a large detector distance (D = 300mm). (d) Same as (c), but at a small detector distance (D = 50mm)

aperture. For both PH and RS, CNR goes up when the point becomes more eccentric.

Fig. 7 shows the CNR(SNR) gain for volume imaging. The results here are very similar to those for planar imaging. That is, Eq. (15) agrees with FIM for small phantoms (Fig. 7(a)) and large D (Fig. 7(c)), and this gain is again underestimated by Eq. (15) for large objects (Fig. 7(b)) and small D (Fig. 7(d)).

IV. Discussion

There are several approximations in the FBP calculation: 1) The phantom needed to be homogeneous and symmetrical about the spin/rotation axis. 2) The sensivity of RS was assumed to be uniform and the position dependence of the geometric efficiency E_r was ignored (See Appendix-A). 3) To simplify the variance calculation, the measurement of the central detector was used to approximate the measurement of every detector (See Appendix-B for more details). With these approximations, the results from calculation are only valid for the central point of an ideal phantom. Obviously, these approximations are more reasonable for a small phantom or at a large detector distance, therefore Eq. (14) and (15) make better predictions in these two cases. On the other hand, for a large phantom or a small detector distance, the difference between the sensitivity of the central point and that of an eccentric point is no longer negligible. In that case, the average E_r decreases and the variance increases, which leads to the underestimation of the SNR gain.

In Fig. 4 and Fig. 7, the SNR ratio reaches a constant asymptotic value at large D. This value is defined by Eq. (16) or (17), which are valid for $D >> W$.

For volume imaging, the linear relationship between the optimal aperture and the target resolution is object-dependent,

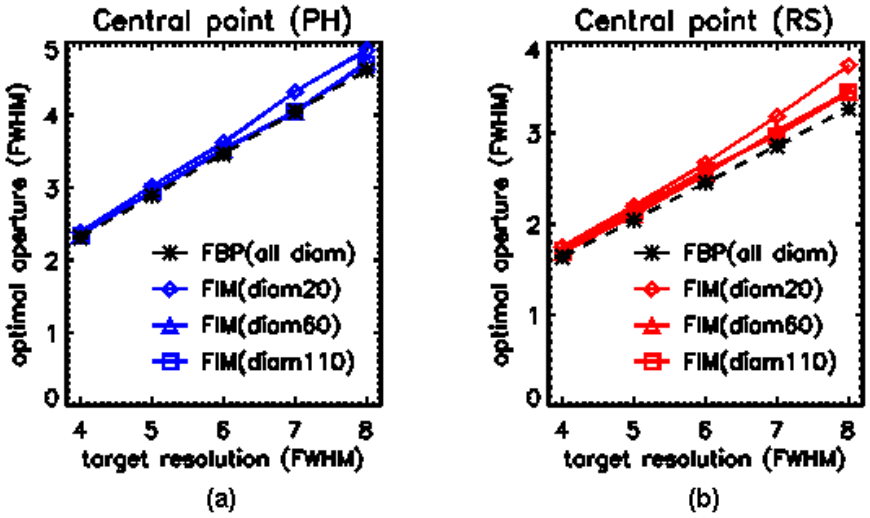

Fig. 5. Comparison between FBP (Eq. (12), (13)) and FIM for the central point of a 3D spherical phantom. Results from FIM were plotted for different phantom sizes (diameter = 20mm, 60mm, 115mm). (a) Optimal collimator aperture for PH. (b) Optimal collimator aperture for RS.

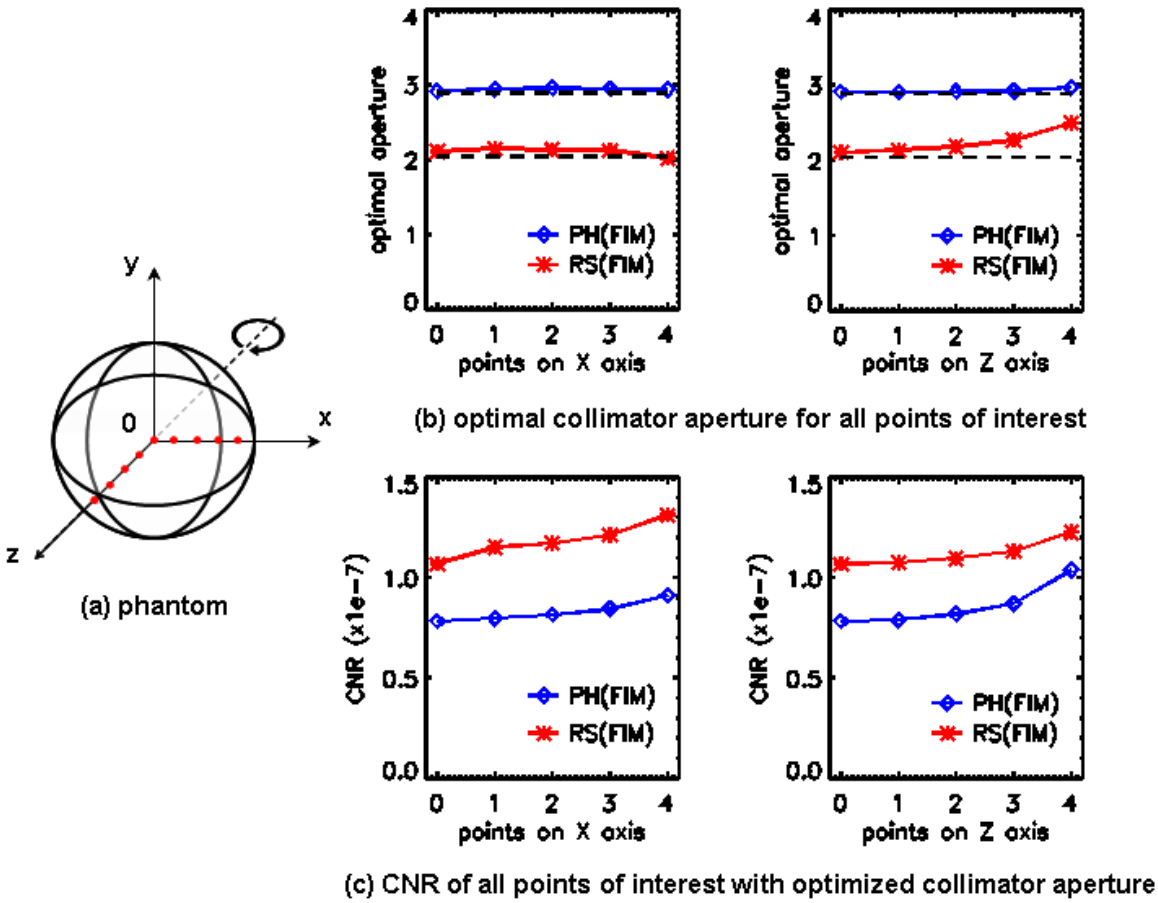

Fig. 6. (a) 3D spherical phantom (diameter = 80mm) and points of interest for volume imaging. z is the axis of rotation. (b) Optimal collimator aperture for all points of interest for a fixed target resolution (FWHM$_t = 5pix$). The dashed lines represent the optimal apertures obtained from the FBP calculation (valid for the central point only). (c) CNR of all points of interest with optimized collimator parameters.

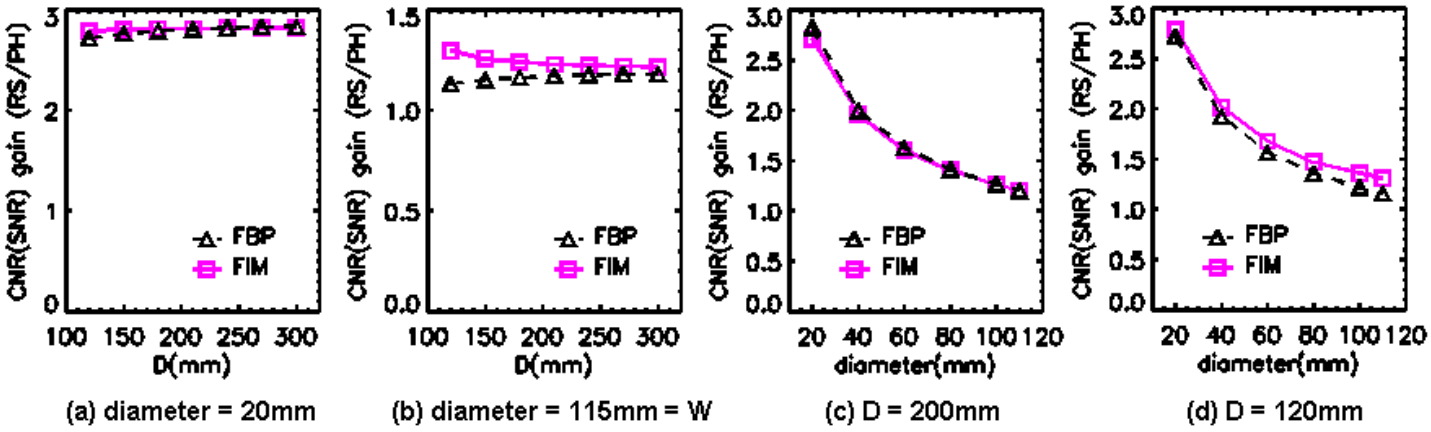

Fig. 7. Comparison between FBP (Eq. (15)) and FIM for volume imaging. (a) CNR(SNR) gain as function of detector distance D for the central point in a small phantom (diameter = 20mm). (b) Same as (a), but for a large phantom (diameter = 115mm = W). (c) CNR(SNR) gain as function of phantom size at a large detector distance (D = 200mm). (d) Same as (c), but at a small detector distance (D = 120mm)

especially for RS (See Fig. 5). However, the CNR versus collimator aperture curve (not shown in this paper), is rather flat near its optimum, which means that CNR is not sensitive to small variations of the collimator aperture near the optimal value. Therefore we still suggest using Eq. (12) and (13) to set the collimator parameters for PH and RS.

For an eccentric point, (at least some of) the RS projections will have a smaller contribution from neighboring activity, when compared to a central point. Consequently, the reconstruction of the eccentric pixel will have a lower variance and higher CNR. The same is true for volume imaging with PH (Fig. 3 and Fig. 6).

The SNR gain Eq. (14) and (15) can also be written as a function of the geometric efficiency gain F ($F = E_r/E_p$). For example, for planar imaging, we have:

$$\text{Gain}_{\text{SNR}}^{\text{opt}} = 1.116\sqrt{\frac{\Omega_W}{diameter}} = 1.712\sqrt{\frac{F\sigma_t}{diameter}} \qquad (18)$$

This expression is similar to those presented in several other papers [3], [7]. The main differences between our approach and others' are that we compared PH and RS at a fixed target resolution, and that we used the optimized aperture for each collimator system.

Based on Fig. 4 and Fig. 7, we can evaluate the overall performance for PH and RS for the central point of a symmetrical phantom. With the same detector width W, PH only outperforms RS for a large phantom measured at a small detector distance. In all other cases, RS is better than PH ($\text{Gain}_{\text{SNR}} > 1$), especially for a small phantom measured at a large detector distance. The results are in agreement with [8].

Up till now, we only investigated points of interest. Actually, the same approach with FIM can also be applied for a region of interest (ROI), which will be done in the future. If RS behaves systematically better than PH for the certain cases, then it is safe to draw a final conclusion.

V. Conclusion

The goal of our study was to compare PH and RS collimators at a matched spatial resolution. Two analytical methods, FBP-based calculation and a Fisher information-based method, were applied to compute the ratio of the SNR of both systems, using a simplified collimator blurring model. It is shown that the two methods yield very similar results for the central point in a uniform disk or sphere phantom. In contrast to the FBP calculation, FIM can predict the LLIR and variance of any pixel of interest in arbitrary non-uniform phantoms. In addition, FIM can be applied with a more realistic collimation model.

Due to the increased noise propagation, RS always needs more post-smoothing than PH. Therefore, for a matched spatial resolution, the collimator resolution of RS should be smaller than that of PH. For the central point of a symmetrical uniform phantom, PH only outperforms RS for large objects at small detector distances, while RS has better SNR in all other cases.

Acknowledgment

The authors wish to thank Roel Van Holen (ELIS, Ghent University) for many useful discussions about the rotating slat collimator systems.

Appendix

A. Geometric Efficiency

The geometric efficiency of a PH collimator is defined as:

$$E_p = \frac{d^2}{4\pi h_p^2} = \frac{\text{FWHM}^2}{4\pi D^2} = \frac{8\ln 2\sigma_p^2}{4\pi D^2} \qquad (19)$$

For the central point of the phantom, the geometric efficiency

of a RS collimator is defined as:

$$\begin{aligned} E_r &= \int_{-W/2}^{+W/2} \frac{d}{4\pi D h_r} \cos^3\beta(x) dx \\ &= \frac{\text{FWHM}}{4\pi D^2} \int_{-W/2}^{+W/2} \cos^3\beta(x) dx \\ &= \frac{\sqrt{8\ln 2}\sigma_r}{4\pi D^2} \Omega_W \end{aligned} \tag{20}$$

with

$$\cos\beta(x) = \frac{D}{\sqrt{x^2+D^2}} \tag{21}$$

For further calculation of Ω_W, let's define $r = \sqrt{x^2+D^2}$. With $\int dx/r^3 = x/D^2 r$, we can derive an analytical expression for Eq. (8):

$$\Omega_W = \int_{-W/2}^{W/2} \frac{D^3}{r^3} dx = \frac{DW}{\sqrt{D^2+W^2/4}} \tag{22}$$

If $D >> W$, then we have:

$$\Omega_W \approx W \tag{23}$$

B. FBP Calculation for Planar Imaging

Here we give the specific calculation steps for planar imaging. For a 2D flat disk phantom $f(\vec{x})$, the measurement of PH (m_p) can simply be modeled as a convolution between $f(\vec{x})$ and a 2D Gaussian PSF with standard deviation σ_p. The measurement of RS (m_r) can be described as a convolution between the ideal 2D Radon transform of $f(\vec{x})$ and a 1D Gaussian PSF with standard deviation σ_r. The measurements are scaled by the geometric efficiency E and the acquisition time T:

$$m_p(\vec{x}) = E_p \times T_p \times \big(f(\vec{x}) \otimes G_2(\vec{x}, \sigma_p)\big) \tag{24}$$

$$m_r(s,\theta) = E_r \times T_r \times \big(m_{r0}(s,\theta) \otimes G_1(s, \sigma_r)\big) \tag{25}$$

where $\theta \in [0,\pi]$ denotes the angular position of the RS collimator as it spins on the fixed camera, and s is the distance between the slat and the spin axis on the gamma camera. $\otimes$ represents the convolution calculation, and G_i denotes the ith-dimensional Gaussian functions:

$$G_i(x_1, x_2, \cdots, x_i, \sigma) = \frac{1}{(\sqrt{2\pi}\sigma)^i} e^{-(x_1^2+x_2^2+\cdots+x_i^2)/2\sigma^2} \tag{26}$$

The definition of E_p and E_r can be found in Appendix-A. For the total acquisition time T, since PH is stationary and RS needs to spin over π, T_p and T_r should be:

$$T_p = T \tag{27}$$

$$T_r = T d\theta/\pi \tag{28}$$

m_{r0} is the ideal unblurred 2D Radon transform of $f(\vec{x})$:

$$m_{r0}(s,\theta) = \int_{\mathbb{R}^2} d\vec{x} f(\vec{x}) \delta(\vec{x}\cdot\vec{u}(\theta) - s) \tag{29}$$

$\vec{u}(\theta) = (-\sin\theta, \cos\theta)$ is the unit vector orthogonal to the slats in the detector plane.

We assume the noise on the measurement is Poisson noise. Hence, the covariance in the measurement is:

$$Cov(m_p(\vec{x}), m_p(\vec{y})) = m_p(\vec{x})\delta(\vec{x}-\vec{y}) \tag{30}$$

$$Cov(m_r(s,\theta), m_r(s',\theta')) = m_r(s,\theta)\delta(s-s')\delta(\theta-\theta') \tag{31}$$

To reconstruct the image for PH, the effect of σ_p is deblurred before post-smoothing the image to yield the fixed TR σ_t. For RS, we process the data in the same way as for PH, and then do the filtered-backprojection. The data processing is done in the Fourier domain. The reconstruction images f_{tp}, f_{tr} in the spatial domain can be described as:

$$f_{tp}(\vec{x}) = \frac{1}{E_p T_p} \times \big(m_p(\vec{x}) \otimes G_2(\vec{x}, \sqrt{\sigma_t^2 - \sigma_p^2})\big) \tag{32}$$

$$f_{tr}(\vec{x}) = \frac{1}{E_r T_r} \int_0^\pi d\theta\, m_r(s,\theta) \otimes h(s) \tag{33}$$

with:

$$h(s) = \int_{\mathbb{R}} dv |v| e^{-2\pi^2(\sigma_t^2-\sigma_r^2)v^2} e^{+2\pi i v s} \tag{34}$$

where v is the frequency conjugate to the sinogram variable s. The variance of the PH estimate $f_{tp}(\vec{x})$ is

$$\begin{aligned} Var(f_{tp}(\vec{x})) &= \frac{1}{(E_p T_p)^2} \int_{\mathbb{R}^2} d\vec{y} \int_{\mathbb{R}^2} d\vec{z}\, G_2(\vec{y}, \sqrt{\sigma_t^2-\sigma_p^2}) \\ &\quad \times G_2(\vec{z}, \sqrt{\sigma_t^2-\sigma_p^2}) Cov(m_p(\vec{x}-\vec{y}), m_p(\vec{x}-\vec{z})) \\ &= \frac{1}{(E_p T_p)^2} \Big(G_2(\vec{x}, \sqrt{\sigma_t^2-\sigma_p^2})\Big)^2 \otimes m_p(\vec{x}) \end{aligned} \tag{35}$$

The variance of the RS estimate $f_{tr}(\vec{x})$ is

$$\begin{aligned} Var(f_{tr}(\vec{x})) &= \frac{1}{(E_r T_r)^2} \int_0^\pi d\theta \int_{\mathbb{R}} ds \int_0^\pi d\theta' \int_{\mathbb{R}} ds' h(s) h(s') \\ &\quad \times Cov(m_r(\vec{x}\cdot\vec{u}(\theta) - s, \theta), m_r(\vec{x}\cdot\vec{u}(\theta') - s', \theta')) \\ &= \frac{1}{(E_r T_r)^2} \int_0^\pi d\theta\, |h(s)|^2 \otimes m_r(s,\theta) \end{aligned} \tag{36}$$

We assume the activity in $f(\vec{x})$ is λ/sec. We approximate the measurement of each point by the measurement of the central point:

$$m_p(\vec{x}) \approx \lambda \times E_p \times T_p \tag{37}$$

$$m_r(s,\theta) \approx \lambda \times E_r \times T_r \times diameter \tag{38}$$

And the variance becomes:

$$\begin{aligned} Var(f_{tp}(\vec{x})) &\approx \frac{\lambda}{E_p T_p} \times \frac{1}{4\pi(\sigma_t^2-\sigma_p^2)} \\ &= \frac{D^2\lambda}{8\ln 2 T \sigma_p^2(\sigma_t^2-\sigma_p^2)} \end{aligned} \tag{39}$$

$$\begin{aligned} Var(f_{tr}(\vec{x})) &\approx \frac{\lambda \times diameter}{E_r T_r} \times \frac{\pi^{-3/2}}{16(\sigma_t{}^2 - \sigma_r^2)^{3/2}} \\ &= \frac{\sqrt{\pi} D^2 \lambda \times diameter}{8\sqrt{2\ln 2}\Omega_W T \sigma_r (\sigma_t{}^2 - \sigma_r^2)^{3/2}} \end{aligned} \tag{40}$$

We can find the minimal variance by deriving the denominator in (39) and (40) with respect to σ_p and σ_r, respectively. The optimal collimator aperture thus is:

$$\sigma_p^{opt} = \sigma_t/\sqrt{2}$$
$$\sigma_r^{opt} = \sigma_t/2$$

With these optimal apertures, the minimal variance for the collimators yields:

$$Var_p^{min} = \frac{D^2\lambda}{2\ln 2 T\sigma_t^4} \quad (41)$$

$$Var_r^{min} = \frac{2\sqrt{\pi}D^2\lambda\times diameter}{3\sqrt{6\ln 2}\Omega_W T\sigma_t^4} \quad (42)$$

The optimized SNR gain for the central point thus is:

$$\begin{aligned}\text{Gain}_{\text{SNR}}^{\text{opt}} &= \sqrt{\frac{Var_p^{min}}{Var_r^{min}}} \\ &= \frac{3^{3/4}}{(8\ln 2\times\pi)^{1/4}} \times \sqrt{\frac{\Omega_W}{diameter}} \\ &= 1.116\sqrt{\frac{\Omega_W}{diameter}}\end{aligned} \quad (43)$$

C. FBP Calculation for Volume Imaging

Here we just give very brief calculation steps. For volume imaging, the collimator and the gamma camera rotate around the z axis $\vec{l_z}$ to obtain the complete tomographic data. For PH, the measurement is denoted as $m(\theta, s, z)$ where z is the axial coordinate of a slice, and s and θ are the usual sinogram coordinates in that slice. For RS, the measurement is parametrized as $m(\phi, s, \theta)$, where ϕ is the rotational position of the camera around the z axis, θ is the rotational position of the collimator as it spins on the fixed camera, and s is the distance between the slat and the collimator spinning axis.

$$m_p(\theta, s, z) = E_p\times T_p\times\big(m_{p0}(\theta, s, z)\otimes G_2(s, z, \sigma_p)\big) \quad (44)$$
$$m_r(\phi, s, \theta) = E_r\times T_r\times\big(m_{r0}(\phi, s, \theta)\otimes G_1(s, \sigma_r)\big) \quad (45)$$

$m_{p0}(\theta, s, z)$ denotes the unblurred 2D Radon transform of $f(\vec{x}) = f(x, y, z)$ in slice z:

$$m_{p0}(\theta, s, z) = \int_{\mathbb{R}^3} d\vec{x} f(\vec{x})\delta(\vec{x}\cdot\vec{l_z} - z)\delta(s - \vec{x}\cdot\vec{u}_p) \quad (46)$$

with

$$\vec{u}_p(\theta) = (-\sin\theta, \cos\theta, 0) \quad (47)$$

$m_{r0}(\phi, s, \theta)$ denotes the ideal 3D Radon transform of $f(\vec{x})$ over the plane $\pi(\vec{u}(\phi, \theta), s)$ that is located at a distance s from the origin of the 3D coordinate system and orthogonal to a unit vector $\vec{u}_r$:

$$m_{r0}(\phi, s, \theta) = \int_{\mathbb{R}^3} d\vec{x} f(\vec{x})\delta(\vec{x}\cdot\vec{u}_r - s) \quad (48)$$

with

$$\vec{u}_r = (-\sin\theta\sin\phi, \sin\theta\cos\phi, \cos\theta) \quad (49)$$

The reconstruction images are

$$f_{tp}(\vec{x}) = \frac{1}{E_p T_p}\int_0^{\pi} d\theta\, m_p(\theta, s, z)\otimes h_p(s, z) \quad (50)$$

$$f_{tr}(\vec{x}) = \frac{1}{2E_r T_r}\int_0^{2\pi} d\phi \int_{-1}^{1} d\cos\theta\, h_r(s)\otimes m_r(\phi, s, \theta) \quad (51)$$

with

$$h_p(s, z) = \int_{\mathbb{R}} dv \int_{\mathbb{R}} dv_z |v| e^{-2\pi^2(\sigma_t^2 - \sigma_p^2)(v^2 + v_z^2)} e^{+2\pi i(vs + v_z z)} \quad (52)$$

$$h_r(s) = \int_{\mathbb{R}} dv v^2 e^{-2\pi^2(\sigma_t^2 - \sigma_r^2)v^2} e^{+2\pi i v s} \quad (53)$$

For the variance calculation, similar approximations are made for the measurements:

$$m_p(\theta, s, z) \approx \lambda\times E_p\times T_p\times diameter \quad (54)$$
$$m_r(\phi, s, \theta) \approx \lambda\times E_r\times T_r\times\pi(diameter/2)^2 \quad (55)$$

Following the same thoughts as for planar imaging, we can derive the expressions for the variance in the reconstructions:

$$Var(f_{tp}(\vec{x})) = \frac{D^2\lambda\times diameter}{64\ln 2 T\sigma_p^2(\sigma_t^2 - \sigma_p^2)^2} \quad (56)$$

$$Var(f_{tr}(\vec{x})) = \frac{3\pi^{3/2}D^2\lambda\times diameter^2}{256\sqrt{8\ln 2}\Omega_W T\sigma_r(\sigma_t^2 - \sigma_r^2)^{5/2}} \quad (57)$$

The optimal collimator aperture can be easily calculated from Eq. (56) and (57):

$$\sigma_p^{opt} = \sigma_t/\sqrt{3}$$
$$\sigma_r^{opt} = \sigma_t/\sqrt{6}$$

Hence, the minimal variance is

$$Var_p^{min} = \frac{27D^2\lambda\times diameter}{256\ln 2\sigma_t^6} \quad (58)$$

$$Var_r^{min} = \frac{81\pi^{3/2}D^2\lambda\times diameter^2}{1600\sqrt{10\ln 2}\Omega_W T\sigma_t^6} \quad (59)$$

The optimized SNR gain for volume imaging is

$$\begin{aligned}\text{Gain}_{\text{SNR}}^{\text{opt}} &= \sqrt{\frac{Var_p^{min}}{Var_r^{min}}} \\ &= \frac{5^{5/4}}{3^{1/2}\pi^{3/4}(8\ln 2)^{1/4}} \times \sqrt{\frac{\Omega_W}{diameter}} \\ &= 1.192\sqrt{\frac{\Omega_W}{diameter}}\end{aligned} \quad (60)$$

REFERENCES

[1] D. Gagnon, G. L. Zeng, J. M. Links, J. J. Griesmer, F. C. Valentino, "Design Considerations for a New Solid-State Gamma-Camera SOLSTICE" *2001 IEEE Nuclear Science Symposium Conference Record*, 2, pp. 1156-1160, 2001

[2] M. A. Lodge, D. M. Binnie, M. A. Flower and S. Webb, "The experiment evaluation of a prototype rotating slat collimator for gamma camera imaging" *Phy. Med. Biol.*, 40, pp. 427-448, 1995.

[3] M. A. Lodge, S. Webb, M. A. Flower and D. M. Binnie, "A prototype rotating slat collimator for single photon emission computed tomography." *IEEE Trans. Med. Imag.*, 15(4), pp. 500-511, 1996.
[4] J. A. Fessler and W. L. Rogers, "Spatial resolution properties of penalized likelihood image reconstruction: space-invariant tomographs." *IEEE Trans. Image Proc.*, 5(9), pp. 1346-1358, 1996.
[5] J. Qi and R. M. Leahy, "Resolution and noise properties of MAP reconstruction for fully 3-D PET." *IEEE Trans. Med. Imag.*, 19(5), pp. 493-506, 2000.
[6] K. Vunckx, D. Bequé, M. Defrise and J. Nuyts, "Single and multipinhole collimator design evaluation method for small animal SPECT." *IEEE Trans. Med. Imag.*, 27(1), pp. 36-46, 2008
[7] B. Zhang and G. L. Zeng, "Study of noise propagation and the effects of insufficient numbers of projection angles and detector samplings for iterative reconstruction using planar-integral data." *Med. Phys.*, 33(9), pp. 3124-3134, 2006.
[8] R. Van Holen, S. Vandenberghe, S. Staelens and I. Lemahieu, "Comparing planar image quality of rotating slat and parallel hole collimation: influence of system modeling." *Phys. Med. Biol.*, 53, pp. 1989-2002, 2008.